

2MASS TWO-COLOR INTERSTELLAR REDDENING LINES IN THE INNER GALAXY

V. Straizys and V. Laugalys

*Institute of Theoretical Physics and Astronomy, Vilnius University,
Goštauto 12, Vilnius LT-01108, Lithuania; strazys@itpa.lt*

Received: 2008 November 2; accepted: 2008 December 15

Abstract. The slopes of interstellar reddening lines in the 2MASS $J-H$ vs. $H-K_s$ diagram for 26 areas in the inner Galaxy (from Vulpecula to Centaurus) are determined. For this aim we use the red-clump giants located inside and behind spiral arms, or behind dense dust clouds of the Local arm. In most of the investigated directions the ratio E_{J-H}/E_{H-K_s} is found to be between 1.9 and 2.0, taking the stars with the extinction $A_V < 12$ mag. The stars with larger extinction deviate down from the reddening lines corresponding to less reddened stars. Probably, this is related to the curvature of reddening lines due to the band-width effect. However, some of the deviating stars may be heavily reddened oxygen- and carbon-rich AGB stars (giants of the latest M subclasses or N-type carbon stars), and pre-main-sequence objects (YSOs).

Key words: ISM: extinction, clouds – stars: fundamental parameters – photometric systems: infrared, 2MASS

1. INTRODUCTION

In the previous paper (Straizys et al. 2008, hereafter Paper I) we have shown that in the direction of the North America and Pelican Nebulae and the Cyg OB2 association the ratio of color excesses E_{J-H}/E_{H-K_s} is close to 2.0, i.e., it is larger than the ‘typical’ value of 1.7–1.8 which follows from the standard interstellar extinction law. Similar values have been obtained by Racca et al. (2002) in the Coalsack and Hoffmeister et al. (2008) in the M 17 nebula. This result stimulated verification of the ratio of 2MASS color excesses in other directions, including dust clouds in the Local arm and more distant clouds. In the present paper we report the results obtained in the direction of the inner Galaxy, between $\ell = 60^\circ$ (Vulpecula) and 310° (Centaurus). The covered areas include both distant clouds in the Sagittarius, Scutum and Norma arms and the Galactic bulge/bar, and the Gould Belt clouds close to the Sun in Aquila, Serpens, Ophiuchus, Scorpius, Sagittarius, Corona Australis and Lupus.

2. THE INVESTIGATED AREAS

The areas for the determination of the ratio of color excesses were selected in Region 1 of the Dobashi et al. (2005) atlas. Two types of areas were taken: (1) the areas located on the Galactic equator every 10 degrees; (2) the densest parts of dust clouds of the Local arm belonging to the Gould Belt. All areas are round with a diameter of 1° . The lists of the areas are given in Tables 1 and 2. In Figure 1 the areas are plotted on the map of Region 1 (Dobashi et al. 2005).

The infrared sources were selected from the 2MASS point-source catalog (Cutri et al. 2006; Skrutskie et al. 2006) taking the J , H and K_s magnitudes with the errors ≤ 0.03 mag.

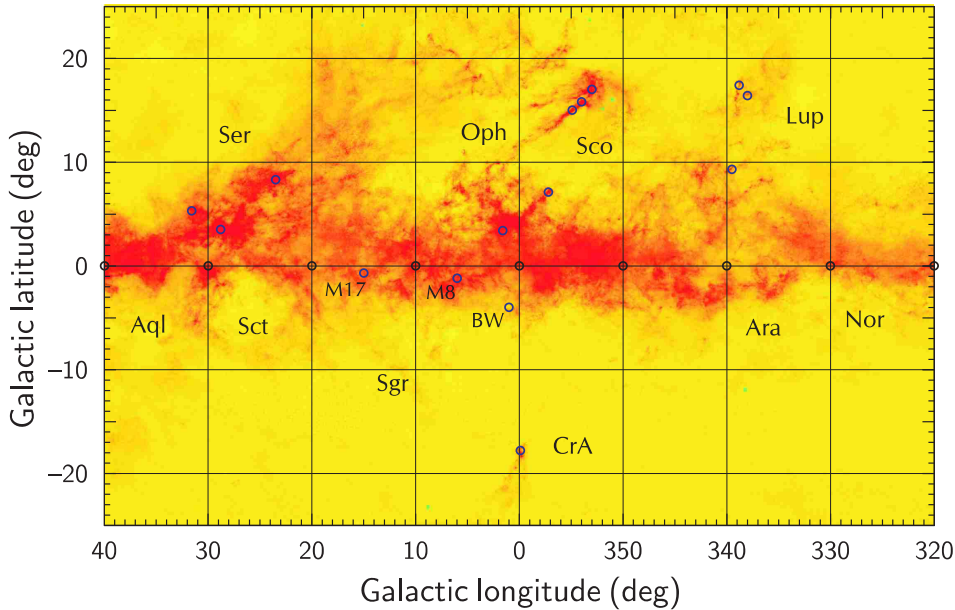


Fig. 1. The investigated areas plotted on the map of dust clouds from Dobashi et al. (2005). Two areas on the Galactic equator at $\ell = 60^\circ$ and 310° are outside the map. BW means Baade's Window.

3. THE METHOD

The majority of stars, located behind a dense dust cloud or a group of clouds, in the $J-H$ vs. $H-K_s$ diagram form a feature similar to a cometary tail. The main constituent of the tail are K and M giants located at different distances and reddened by dust clouds distributed along the line of sight. Among these stars, the red clump giants (hereafter RCGs) of spectral type $\sim K2$ III are most abundant. Their absolute magnitude in the K_s passband, M_{K_s} , is close to -1.6 (Alves 2000; Grocholski & Sarajedini 2002; Groenewegen 2008).

The upper edge of this tail usually is much sharper than the lower edge where a large variety of objects with different interstellar reddenings can be present. These objects can belong to the following types: (1) AGB stars, including the coolest M-type giants, oxygen- and carbon-rich long-period variables, OH/IR stars; (2) young

stellar objects (YSOs), including Orion-type variables and Herbig Ae/Be stars in different stages of evolution; (3) ordinary Be-type stars with gas envelopes; (4) point-like galaxies and quasars. Sometimes these objects form the second tail which usually is broader than the upper one (see Straizys & Laugalys 2007). If the dust cloud (or other clouds behind it) does not show star-forming activity, the YSOs are absent. Galaxies, quasars and Be stars usually are not numerous. Consequently, the objects scattered along the lower edge of the main ‘tail’ in many cases are cool AGB stars only.

For determining the reddening line slope (i.e., the ratio E_{J-H}/E_{H-K_s}) we applied the method described in Paper I, Section 5. It is based on using the tail formed by reddened RCGs, scattered around a line crossing their intrinsic position at $J-H = 0.60$ and $H-K_s = 0.15$. The only difference is that in Paper I we used a little different intrinsic position of RCGs determined for the clump stars in the open cluster M 67. Now it is evident that M 67 RCGs are too hot (spectral types G8–K0 III) comparing to the majority of the field RCGs which are mostly of spectral types closer to K2 III.

Although the number of RCGs exceeds considerably the number of stars which in the color-magnitude diagram lie on the sequence of red giants, most of them in the $J-H$ vs. $H-K_s$ diagram form a common reddening line since their intrinsic line almost coincides with the direction of the reddening line. Only the giants of spectral types later than M5 III (most of them are asymptotic-branch giants) deviate down from the G8–M5 giant sequence (see Figure 4b). Consequently, we are free to consider that all giants from G8 to M5 in the $J-H$ vs. $H-K_s$ diagram form a common reddening line of red giant branch.

To make the estimation of the reddening line slope easier, in the $J-H$ vs. $H-K_s$ diagram of each area a fan of reddening lines of RCGs with the slopes between 1.7 and 2.2 were drawn. The optimum slope for each area was determined by taking the average of slopes of individual reddening lines for stars with color indices $J-H$ between 1.8 and 2.2. We have avoided cooler stars since the reddening lines exhibit curvature due to the band-width effect.

In the following we accept the location of spiral arms according to the Vallee (2005) four-arm model. The recent model of Benjamin et al. (2008) accepting two star-rich arms and two star-poor arms, based on the *Spitzer* GLIMPSE project, does not change the positions of spiral arms close to the Sun. Consequently, the main results of our study remain valid in both models. We accept that in the Galactic center direction the heliocentric distance of the Sagittarius arm is 1–2 kpc and of the Scutum arm it is 2.5–3.5 kpc.

4. RESULTS

A general feature in $J-H$ vs. $H-K_s$ diagrams for most of the areas is an uneven distribution of stars along the reddening line of red giants. The presence of clumps or density jumps at certain color excesses is related to the distribution of interstellar dust clouds along the line of sight. Usually, the dust density is the largest inside spiral arms. The distribution of density jumps in the $J-H$ vs. $H-K_s$ diagram can be better understood analyzing the distribution of stars in corresponding K_s vs. $H-K_s$ color-magnitude diagrams (hereafter CMD). In Figures 2 and 3 two typical diagrams for the areas on the Galactic equator at $\ell = 50^\circ$ (in Aquila) and $\ell = 2.5^\circ$ (close to the Galactic center) are presented.

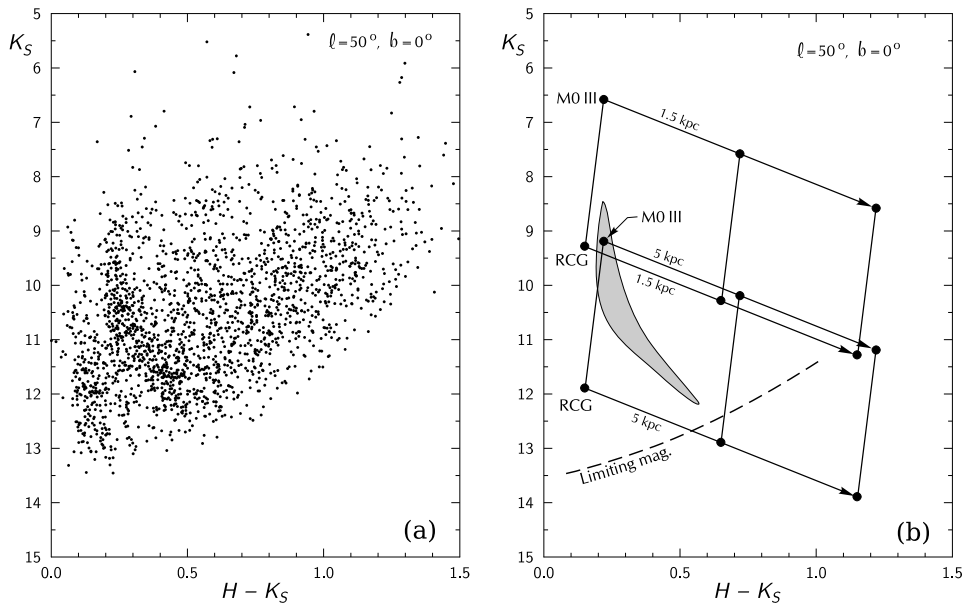


Fig. 2. Color-magnitude diagram K_S vs. $H - K_S$ and its interpretation in the direction of $l = 50^\circ, b = 0^\circ$ in Aquila.

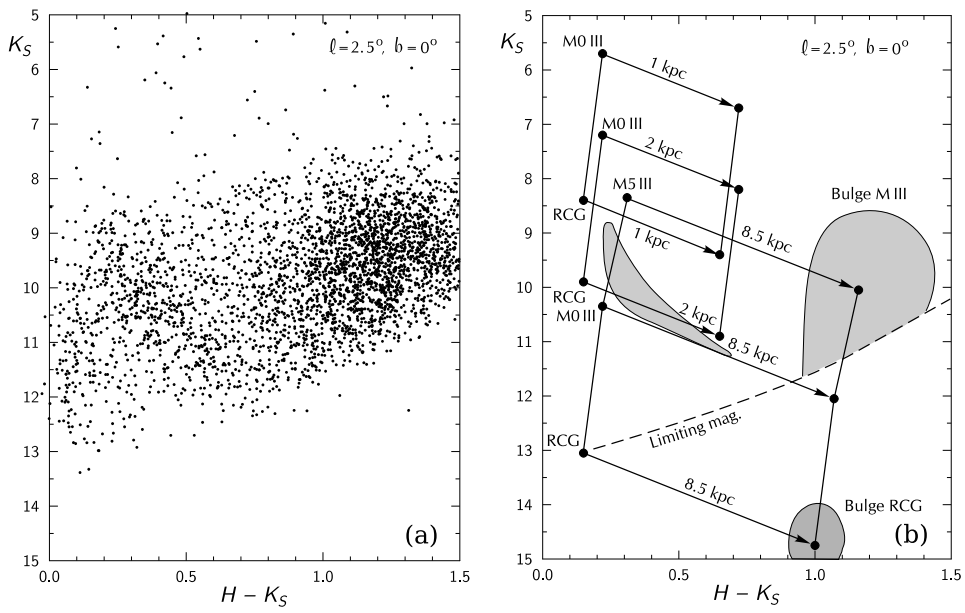


Fig. 3. Color-magnitude diagram K_S vs. $H - K_S$ and its interpretation in the direction of $l = 2.5^\circ, b = 0^\circ$ at the Galactic center.

4.1. Color-magnitude diagram along the Sagittarius arm

In the area at $\ell = 50^\circ$ within the heliocentric distance of 2–5 kpc the line of sight runs along the Sagittarius arm. In Figure 2 the left panel is plotted for the 2MASS data while the right panel gives a schematic explanation of the features observed. The positions of the unreddened and reddened by $E_{H-K_s} = 0.5$ and 1.0 stars for RCGs and M0 III giants at distances of 1.5 and 5 kpc, joined by solid lines, are shown. These color excesses correspond to $A_V = 8.5$ and 17.0 mag. The slope of the reddening line, or the ratio A_{K_s}/E_{H-K_s} is accepted to be 2.0. The broken line at the bottom shows the limiting 2MASS K_s magnitudes at which the accuracy of photometry in all three passbands is ≤ 0.03 mag.

The most conspicuous feature in the diagram is the sequence of stars running from $(K_s, H-K_s) = (8.5, 0.22)$ to $(12.2, 0.6)$. This sequence corresponds to RCGs of spectral types K0–K3 III located in front of the Sagittarius arm (upper end) and within the arm. In this direction the space density of RCGs with distance should be more or less constant, but due to increasing volume of space at larger distances the surface density of stars increases. The width of the RCG sequence is defined by the presence of cloud clumps and windows in the arm.

In Figure 2 the RCG sequence appears at a distance of about 1 kpc where the cone with a diameter of 1° counts up a sufficient number of RCGs at $(K_s, H-K_s) = (8.5, 0.22)$. These stars are already reddened with $E_{H-K_s} \approx 0.07$ ($A_V = 1.2$ mag) by the Aquila Rift dust clouds located at a distance of ~ 200 – 300 pc (Straizys et al. 1996, 2003; Eiroa et al. 2008; Prato et al. 2008). Between the Local and the Sagittarius arms the reddening should be small. Therefore at the beginning the RCG sequence runs almost vertically down due to increasing distance. At ~ 2 kpc ($K_s = 10.2$) the sequence turns to right forming a curve running down to the end at $(K_s, H-K_s) = (12.2, 0.6)$ where the line of sight leaves the Sagittarius arm. At larger distances the line should fall more or less vertically down before the Perseus arm is reached. However, this extension of the line is not seen due to the limiting magnitude.

The dust in a spiral arm shifts along the reddening line not only RCGs, but all the red giant sequence, which extends both down and up from the clump (except RCGs, in Figure 2b we show the positions of M0 III stars). The K3–M5 III stars of the Sagittarius arm fill the region of the CMD above the RCG sequence, with $H-K_s$ approximately between 0.25 and 0.7. M-type giants of late subclasses, located between the Sagittarius and Perseus arms, due to their high luminosity in the K_s passband, also should be present in Figure 2, right of $H-K_s \approx 0.7$.

The stars at the left lower corner of the CMD with $H-K_s < 0.2$ are unreddened or slightly reddened main sequence stars of spectral types A–F–G located up to a distance of ~ 500 pc from the Sun.

4.2. Color-magnitude diagram in the direction of the Galactic bulge

Figure 3a shows the K_s vs. $H-K_s$ diagram at $(\ell, b) = (2.5^\circ, 0^\circ)$, i.e., for a region close to the Galactic center. We have avoided the area placed directly on the center since in it, due to very large interstellar extinction, the distribution of stars is not typical for other areas in the direction of the bulge. In the bulge direction the line of sight crosses the Sagittarius arm and other arms almost perpendicularly.

Figure 3b gives the interpretation of the distribution of stars. Again, as in Figure 2, we see the sequence of RCGs which starts more or less at the same K_s magnitude and $H-K_s$ color with small reddening, $E_{H-K_s} = 0.25$, caused by dust

clouds in the Gould Belt (probably, an extension of the Pipe Nebula cloud). At a distance of 1 kpc the line of sight enters the Sagittarius arm. The RCG sequence is not so steep as at 50° and runs to somewhat larger reddenings (up to $H-K_s = 0.7$). Both these facts mean that the dust concentration in the Sagittarius arm in the direction of the Galactic center is larger than along the arm at the 50° longitude. Also, the RCG sequence in Figure 3 is broader, and this may mean that the extinction in this direction is more spotty. Near the end of the RCG sequence, whose form is defined by the dust distribution in the Sagittarius arm, the giants in the Scutum arm should appear (at about 2.5 kpc). However, in Figure 3 we do not see any signs of the Scutum arm, maybe due to proximity of its RCGs to the limiting magnitude.

In comparison with Figure 2, a new feature appears in the right side of Figure 3 – between $K_s = 8-11$ and $H-K_s = 1.0-1.5$ there is a large clump of stars belonging to the Galactic bulge. As panel 3b explains, this concentration is only a ‘tip of the iceberg’, the long red giant sequence of the bulge, with the reddening $E_{H-K_s} = 0.85$, or the extinction $A_V = 14.5$ mag. Dust clouds responsible for this large reddening are located in the Local, Sagittarius, Scutum, Norma and 3-kpc arms. RCGs on this sequence are located at $K_s = 14.75$, i.e., far below the limiting magnitude. The presence of the clump at approximately this position was confirmed by Nishiyama et al. (2006). This is in accordance with the intrinsic RCG position at $K_s = 13$ mag shown in Figure 3b. This position of RCGs of the bulge was confirmed by Tiede et al. (1995), using *JHK* photometry in Baade’s Window.

Above the CMD limiting magnitude only M giants of the bulge are seen. As follows from Figure 3b, many of them are situated higher than the giants of spectral class M5 III located at a distance of 8.5 kpc. This can be explained by a large radial extent of the bulge which starts at a heliocentric distance of ~ 5 kpc. Also, a part of the bulge stars are cooler and more luminous in K_s than M5, most of them are AGB long-period variables (Schultheis & Glass 2001). Their scatter in CMD can be the result of their variability, presence of warm circumstellar gaseous and dusty envelopes and different interstellar reddenings.

Using the DENIS and 2MASS data, the described M0–M6 giants of the bulge with intrinsic K_s magnitudes between 8 and 12 have been used by Schultheis et al. (1999) and Dutra et al. (2002, 2003) for the extinction investigation in the bulge. The same method, applying the K vs. $J-K$ diagram, was used earlier by Tiede et al. (1995) and Frogel et al. (1999) in the NICMOS 3 (Las Campanas) system.

Figures 2 and 3 show that the presence of interstellar extinction and reddening makes possible to identify giants of different spectral classes belonging to the specific spiral arms and the bulge. Without reddening or with small reddening such possibility vanishes. This is illustrated by the CMD for Baade’s Window, a relatively transparent region ($A_V \approx 1.6$ mag for the globular cluster NGC 6522 seen in the center) in the direction of the Galactic bulge at $\ell = 1^\circ$, $b = -4^\circ$ (Figure 4a). In this diagram the giants located at various distances and belonging to the disk and the bulge form a single band.

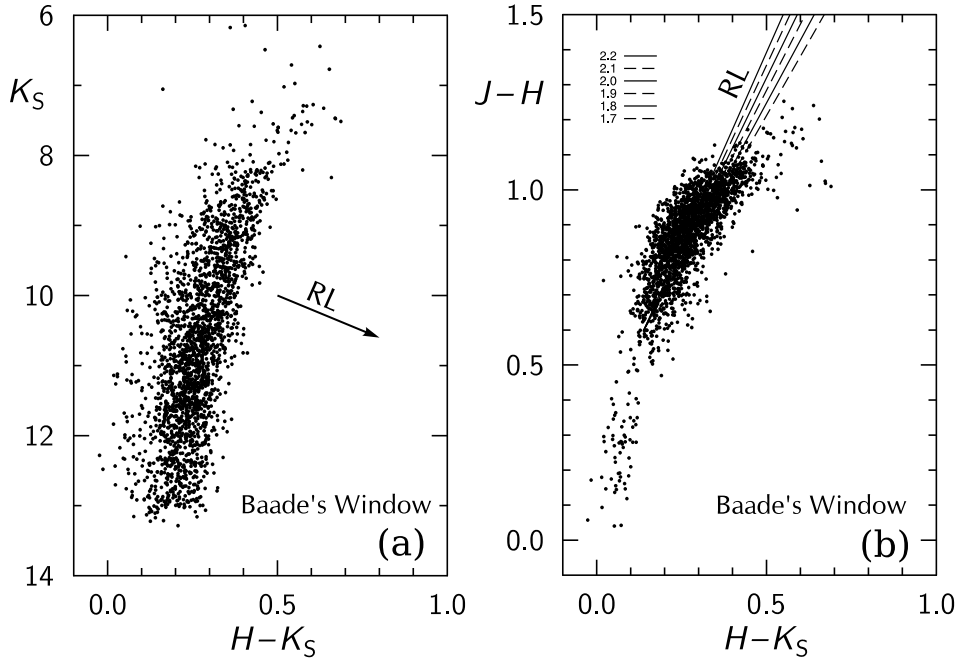


Fig. 4. Color magnitude and two-color diagrams for Baade's Window ($\ell = 1^\circ$, $b = -4^\circ$, diameter $15'$).

Table 1. The investigated areas located on the Galactic equator. The given mean ratios of color excesses correspond to red giant branch stars at $J-H \approx 2.0$. The last column shows the number of stars used to calculate the ratio of color excesses.

Area	Center ℓ° b°	E_{J-H}/E_{H-K_s} at $J-H = 2.0$	Number of stars
Vul (60,0)	60.0 0.0	2.035 ± 0.158	216
Aql (50,0)	50.0 0.0	1.992 ± 0.142	313
Aql (40,0)	40.0 0.0	1.976 ± 0.157	933
Aql/Sct (30,0)	30.0 0.0	1.984 ± 0.156	484
Sct (20,0)	20.0 0.0	1.977 ± 0.152	709
Sgr (10,0)	10.0 0.0	1.935 ± 0.140	557
Sgr (0,0)	0.0 0.0	2.018 ± 0.175	72
Sco (350,0)	350.0 0.0	1.958 ± 0.147	594
Sco/Ara (340,0)	340.0 0.0	1.984 ± 0.168	514
Nor (330,0)	330.0 0.0	1.949 ± 0.132	566
Cir (320,0)	320.0 0.0	1.989 ± 0.145	634
Cen (310,0)	310.0 0.0	2.000 ± 0.144	354

4.3. Two-color diagrams at the Galactic plane

Two-color $J-H$ vs. $H-K_s$ diagrams for the Galactic equator areas between $\ell = 60^\circ$ and 310° at each longitude multiple to 10° are shown in Figures 5 (a-l). The areas are listed in Table 1 with the calculated mean slopes of their reddening

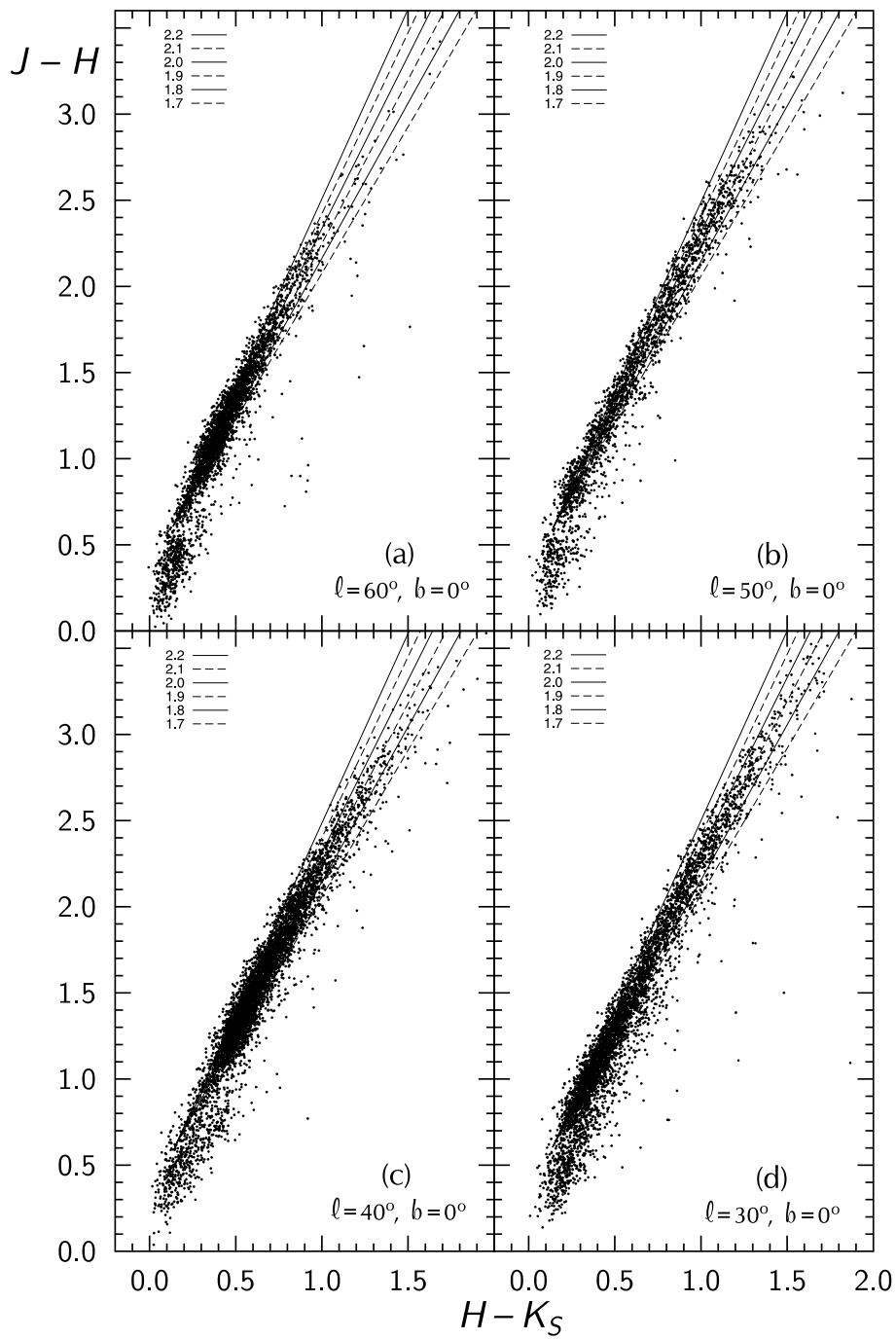


Fig. 5 (a-d). Two-color diagrams for the areas on the Galactic equator at $\ell = 60^\circ, 50^\circ, 40^\circ$ and 30° . The six straight lines are the reddening lines of RCGs with different slopes, explained in the inserts.

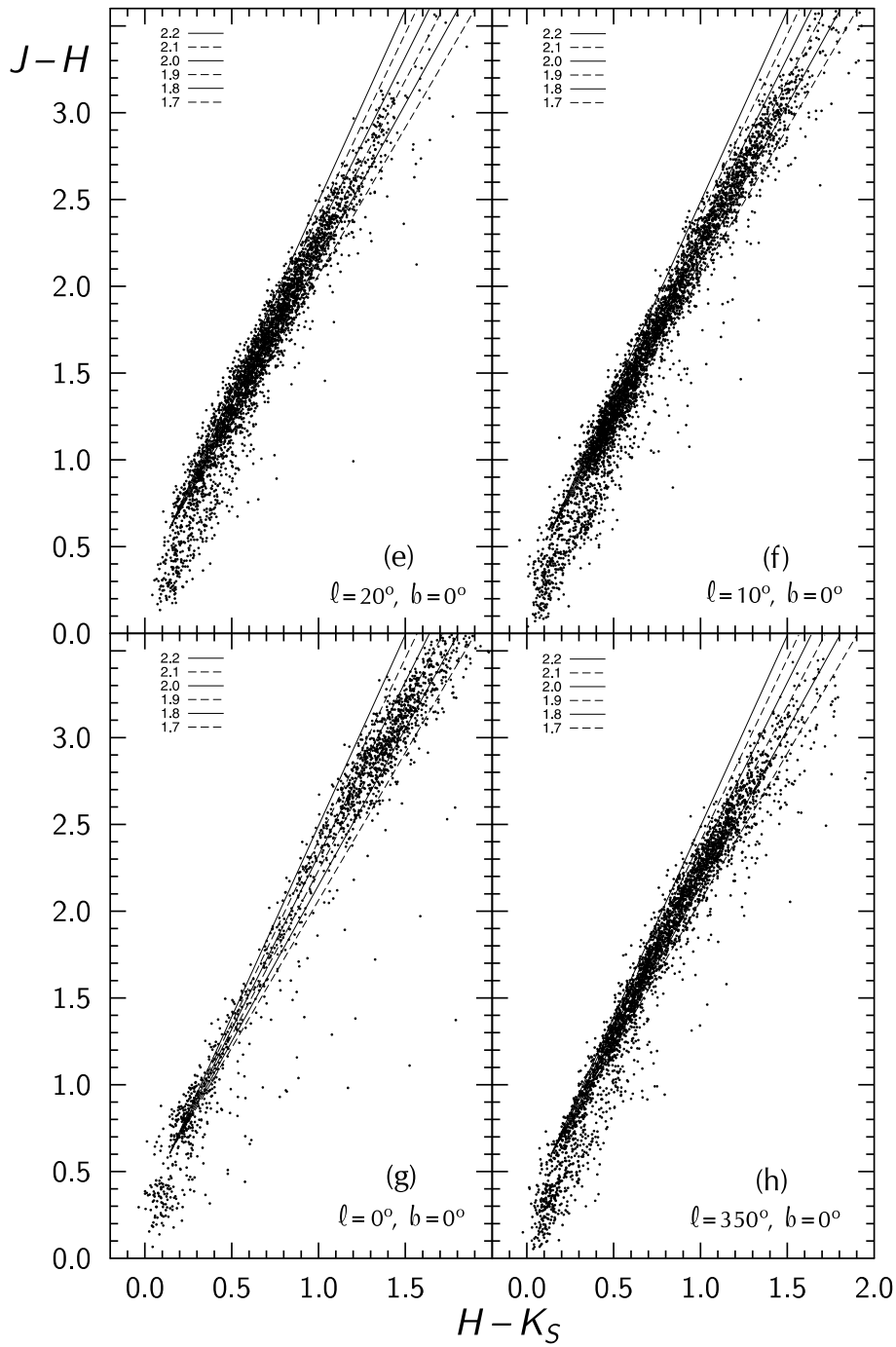


Fig. 5 (e-h). The same as in Fig. 5 (a-d) but for the areas at $\ell = 20^\circ, 10^\circ, 0^\circ$ (Galactic center) and 350° .

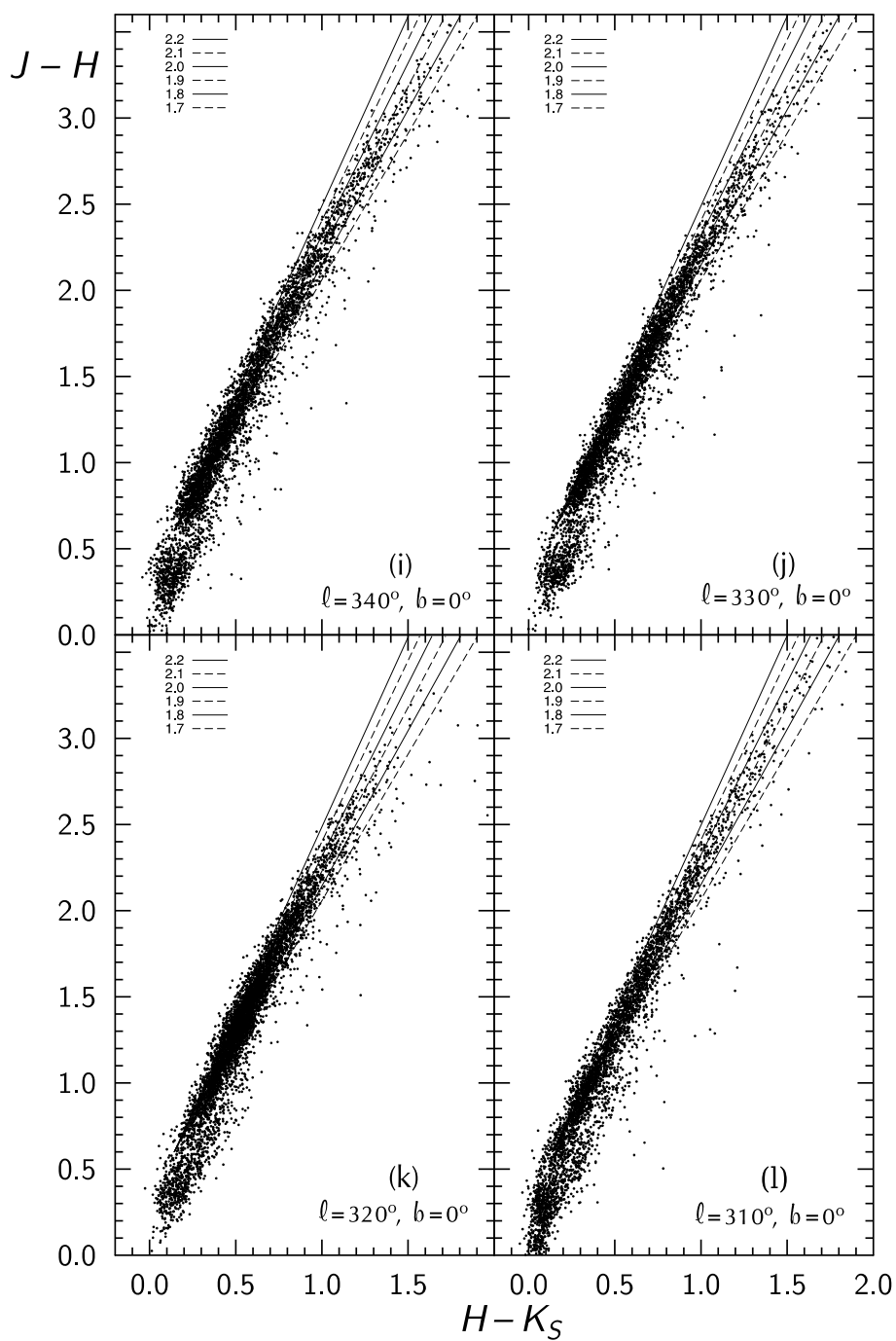


Fig. 5 (i-l). The same as in Fig. 5 (a-d) but for the areas at $\ell = 340^\circ, 330^\circ, 320^\circ$ and 310° .

lines for red giants with $J-H$ between 1.8–2.2. When calculating slopes of the reddening lines, the possible AGB stars and YSOs located below the reddening line of the slope 1.6, have been excluded. In the next we will discuss these diagrams considering both the distribution of stars along reddening lines and the ratios of color excesses in the given directions.

4.3.1. $\ell = 60^\circ$, $b = 0^\circ$

In this direction the line of sight runs along the inner edge of the Local arm, where space is relatively transparent. However, at ~ 400 pc it crosses a dust cloud (hereafter the Vulpecula cloud, Neckel & Klare 1980; Forbes 1985) and at 2–2.5 kpc a cloud inside the Vul OB1 association (Dame & Thaddeus 1985). In the CMD of the area the RCG sequence, corresponding to the Local arm, runs steeply down between $(K_s, H-K_s) = (9.0, 0.2)$ and $(11.0, 0.35)$. At a distance of 5–6 kpc the line of sight enters the branching of the Local and Sagittarius arms. At this distance the RCG sequence should begin at $(K_s, H-K_s) = (12.5, 0.35)$, i.e., very close to the limiting K_s magnitude. Cooler and absolutely brighter stars of the Local arm with various reddenings are seen filling the area between $K_s = 8.0$ and 13.0, with $H-K_s > 0.3$.

In the $J-H$ vs. $H-K_s$ diagram (Figure 5a) the stars with $J-H < 0.6$ all belong to the Local arm and are unreddened or little reddened (up to $E_{H-K_s} \sim 0.1$) main-sequence F–G stars. The stars lying at the lower edge of the reddening line of giants can be B–A–F stars of the Local arm considerably reddened by the Vulpecula cloud and the Vul OB1 association cloud; some of them can be pre-main-sequence stars (YSOs). The stars on the giant sequence with $J-H < 0.9$ correspond to the Local arm in the solar vicinity and the interarm region, while at larger $J-H$ values most stars belong to the intersection of the Local and the Sagittarius arms. Along the reddening line, K and M giants of various spectral subclasses should be mixed together, and the slope of the line is 2.04 ± 0.16 (Table 1).

4.3.2. $\ell = 50^\circ$, $b = 0^\circ$

As was discussed in Section 4.1, this direction coincides with the line of sight along the Sagittarius arm. In the $J-H$ vs. $H-K_s$ diagram (Figure 5b) the reddening line consists mostly of RCGs (and other stars of the red giant branch) located at various distances and reddened by different cloud groups. The RCGs lying lower than $J-H = 1.0$ are affected only by the Local arm clouds. However, the K_s vs. $H-K_s$ diagram (Figure 2) shows that these stars are located in the interarm space, close to the Sagittarius arm (see discussion in Section 4.1). The RCGs with $J-H$ between 1.0 and 1.5 are distributed along the Sagittarius arm. The stars with $J-H > 1.5$ in the CMD all lie above and right of the RCG sequence and should be field giants of spectral types later than K3 III. In Figure 5b the majority of heavily reddened stars are scattered between the reddening lines of the slopes $E_{J-H}/E_{H-K_s} = 1.9$ and 2.1, the mean slope at $J-H = 2.0$ being 1.99 ± 0.14 .

However, the reddest stars exhibit a tendency to deviate down, to the lower values of color-excess ratio. No doubt, this effect is related mainly to the curvature of the reddening lines due to the band-width effect (Straizys & Lazauskaitė 2008). Partly, the location of the reddest stars can be the result of the selection effect caused by bending down of the intrinsic red-giant sequence for spectral types cooler than M6 III (most of them should be long-period variables). In Figure 4b we show the $J-H$ vs. $H-K_s$ diagram for stars located in a semi-transparent area of

a diameter of $15'$ at the Galactic center, in the direction of Baade's Window. The stars near the end of the giant branch with $J-H = 1.0-1.2$, when shifted along the reddening line with the slope ~ 2.0 up to $J-H = 2.5-3.0$, will appear at the position corresponding to the reddening lines of RCGs with the slope $1.6-1.8$. A part of these reddest stars can also be heavily reddened carbon stars since their intrinsic position in the $J-H$ vs. $H-K_s$ diagram is also lower than of M0-M5 III stars. At the end of the reddening line we observe only the coolest oxygen- and carbon-rich AGB stars due to a selection effect: they are seen at larger distances (and higher reddenings) due to higher luminosity. At this distance (and reddening) RCGs apparently are too faint. Therefore, in determining the slope of the reddening line we do not use stars redder than $J-H > 2.2$.

4.3.3. $\ell = 40^\circ, b = 0^\circ$

In this direction the line of sight crosses a quite dark region of the Aquila Rift. In the CMD the RCG sequence shows that the reddening in the Local arm is $E_{H-K_s} \approx 0.15$ or $A_V = 2.5$, i.e., it is larger than at 50° . The Sagittarius arm is crossed twice: between $2.5-3.5$ kpc and at ~ 8 kpc. The largest extinction (up to $A_V \approx 8$) is observed at the far end of the first crossing, at $3.0-3.5$ kpc. In the second crossing of the Sagittarius arm, RCGs are too faint to be visible in K_s . However, M-type giants and carbon stars can be present in the sample.

The diagram $J-H$ vs. $H-K_s$ (Figure 5c) confirms that the reddening in this direction of the Local arm is larger; the concentration of red giants begins at $J-H = 1.1$. The 'tail' formed by reddened stars in the Sagittarius arm is also longer. The distribution of stars at $J-H = 2.0$ is in accordance with the mean reddening line slope of 1.98 ± 0.16 .

4.3.4. $\ell = 30^\circ, b = 0^\circ$

The area is at the Aquila and Scutum border, in the direction of a protrusion of the Aquila Rift. The line of sight, after leaving the Local arm, at a distance of ~ 2 kpc crosses the Sagittarius arm and at a distance 3.5 kpc it enters and runs along the Scutum arm. The Galactic bulge or bar are not reached yet. The CMD of this area is rather complicated, and it is difficult to disentangle the effects of reddening in the Local, Sagittarius and Scutum arms. It seems, however, that the reddening in this direction is larger than at $\ell = 40^\circ$. In the $J-H$ vs. $H-K_s$ diagram (Figure 5d) the mean slope of the reddening line of red giants at $J-H = 2.0$ is 1.98 ± 0.16 .

4.3.5. $\ell = 20^\circ, b = 0^\circ$

The area is in Scutum, at the southern edge of the Aquila Rift. In this direction the line of sight crosses the Sagittarius and Scutum arms and at ~ 5 kpc enters the bulge (including the end of the bar and the beginning of the Near 3-kpc arm). In the CMD the RCG sequence runs from $(K_s, H-K_s) = (9.0, 0.3)$ to $(12.0, 0.6)$, i.e., includes RCGs reddened in the Local, Sagittarius and Scutum arms together. At the same time at $(K_s, H-K_s) = (8.5, 0.9)$ the tip of the sequence of the bulge giants appears. At $(12.0, 0.6)$ it converges with the RCG sequence.

In the $J-H$ vs. $H-K_s$ diagram (Figure 5e) red giants cover the reddening line without jumps, with the largest concentration at $J-H = 1.5$. The stars with redder colors probably all belong to the bulge and are M-type giants. The slope of the reddening line at $J-H = 2.0$ is 1.98 ± 0.15 .

4.3.6. $\ell = 10^\circ$, $b = 0^\circ$

The area is in Sagittarius, between the Small Sagittarius Cloud (M24) and the Trifid Nebula (M20). In this direction the line of sight crosses the Local, Sagittarius and Scutum arms and enters deep into the bulge. In the CMD the RCG sequence is not sufficiently definite, but a dense clump at $(K_s, H-K_s) = (11.0, 0.4)$ is seen. This clump has an extension upward which probably is the red giant sequence reddened by the Local and Sagittarius arms. Also, the area of the bulge M-type giants with larger reddening is seen, but not so concentrated as in the $\ell = 20^\circ$ area.

The $J-H$ vs. $H-K_s$ diagram of the area (Figure 5f) is similar to that at $\ell = 20^\circ$, but the reddening line is much richer at large reddenings. The mean slope of the reddening line at $J-H = 2.0$ is 1.94 ± 0.14 .

4.3.7. $\ell = 0^\circ$, $b = 0^\circ$

This is the area in the direction to the Galactic center. The structure of the CMD in this direction is similar to that for $\ell = 2.5^\circ$ described in Section 4.2 but with some important differences. The number of stars everywhere is much smaller, probably due to large interstellar extinction. The RCG sequence is seen only down to $(K_s, H-K_s) = (11.0, 0.3)$. The RCGs in Sagittarius and Scutum arms between $K_s = 11-13$ are absent; probably, they are reddened so strongly that have been moved down along reddening lines lower than the limiting K_s magnitude. However, the tip of the sequence of bulge M-type giants is well seen at $(K_s, H-K_s) = (9.5, 1.4)$.

The $J-H$ vs. $H-K_s$ diagram of the area (Figure 5g) is also peculiar. The unreddened or little reddened red giants of the Local arm and, maybe, of the beginning of the Sagittarius arm, are seen up to $J-H \approx 1.3$. The bulge M-giants are strongly shifted along the reddening line and their density increases considerably only at $J-H > 2.5$, reaching maximum at about 3.0. The mean reddening of the upper tip of the bulge giant sequence estimated from the CMD is $E_{H-K_s} \approx 1.1$, this corresponds to $A_V = 18.7$ mag. This is the mean value of the extinction over an area of 1° diameter. Some individual stars exhibit $H-K_s \geq 2.0-2.5$, and this corresponds to $A_V \approx 40$ mag. This is in agreement with the results of Schultheis et al. (1999) using the DENIS survey data and Cotera et al. (2000) using the AAS JHK' system.

The mean slope of the reddening line of red giants at $J-H = 2.0$ in the direction of the Galactic center does not differ from other areas discussed above, its value is 2.02 ± 0.18 . The stars with $J-H > 3.0$ deviate down; part of them can be the AGB stars of the bulge (see the discussion in subsection 4.3.2).

4.3.8. $\ell = 350^\circ$, $b = 0^\circ$

The area is in Scorpius, its line of sight crosses the Local, Sagittarius, Scutum, Norma, 3-kpc arms and the bulge. Although the area is symmetrical with respect to the Galactic center to the $\ell = 10^\circ$ area, their CMDs differ considerably. At 350° we see quite distinct RCG sequence consisting of two parts, corresponding probably to the Sagittarius and the Scutum arms: it runs from $(K_s, H-K_s) = (9.0, 0.25)$ to $(11.0, 0.6)$. The upper part of the bulge giant sequence at $(K_s, H-K_s) = (9.5, 1.0)$ is also more populated.

The $J-H$ vs. $H-K_s$ diagram of the area (Figure 5h) is very similar to that for $\ell = 10^\circ$. The only significant difference is that at $\ell = 350^\circ$ the maximum

reddening is smaller. The mean slope of the reddening line of red giants at $J-H = 2.0$ is 1.96 ± 0.15 .

4.3.9. $\ell = 340^\circ$, $b = 0^\circ$

The area is at the Scorpius, Ara and Norma corner. In this direction the line of sight crosses the Local, Sagittarius, Scutum, Norma and 3-kpc arms. However, the distance of the Norma arm is at 5 kpc, i.e., its RCGs are fainter than the limiting magnitude. The CMD of this area, in comparison to the mirror area at $\ell = 20^\circ$, shows the same features, but the RCG sequence corresponding to the Sagittarius and Scutum arms at $\ell = 340^\circ$ is much more populated. This effect could be of instrumental origin if in the southern sky 2MASS magnitudes were measured with higher accuracy. More populated are and other areas of the Southern sky.

The $J-H$ vs. $H-K_s$ diagram of the area (Figure 5i) is more abundant in red giants at low reddenings than the diagram for $\ell = 20^\circ$. Otherwise, both diagrams are similar, exposing the same slope.

4.3.10. $\ell = 330^\circ$, $b = 0^\circ$

The area is projected on one of the dark lanes in Norma. In this direction the line of sight crosses the Local, Sagittarius and Scutum arms and then runs along the Norma arm. In comparison with the area at $\ell = 30^\circ$ on the other side of the Galactic center, its RCG branch in CMD is much more populated and is bluer: it runs from $(K_s, H-K_s) = (9.0, 0.3)$ to $(12.0, 0.6)$. This is seen in the rich $J-H$ vs. $H-K_s$ diagram (Figure 5j) where high concentration of red giants starts at $J-H = 0.75$. All this shows that the extinction in the Norma clouds is much lower than in the Aquila Rift clouds. However, the slope of the reddening line is similar in both directions.

4.3.11. $\ell = 320^\circ$, $b = 0^\circ$

This area is located in the direction of the same Norma dark lane, only 4° from α Cen. The line of sight crosses the Sagittarius and Scutum arms (the last arm twice). CMDs of this area and the mirror area at $\ell = 40^\circ$ are quite similar, but the area of the southern sky is again richer in stars. The reddening in the 320° area is also smaller than in its northern counterpart: the RCG sequence runs from $(K_s, H-K_s) = (9.0, 0.25)$ to $(12.5, 0.6)$. The $J-H$ vs. $H-K_s$ diagrams (Figures 4c and 4k) of both areas are similar, but in the southern area the density of red giants is larger at lower reddenings. The slope of the reddening line at $J-H = 2.0$ is 1.99 ± 0.14 .

4.3.12. $\ell = 310^\circ$, $b = 0^\circ$

This area is located in a relatively transparent direction between the star α Cen and the Coalsack. In this direction, after crossing the Local and Sagittarius arms, the line of sight runs along the Scutum arm. CMD and $J-H$ vs. $H-K_s$ diagrams for this area (Figure 5l) are quite similar to the diagrams for its mirror area in the northern sky at $\ell = 50^\circ$ (Figures 2a and 5b), however, the 310° area contains many more stars, as the other southern areas. In the CMD the RCG sequence extends from $(K_s, H-K_s) = (9.0, 0.2)$ to $(12.3, 0.65)$, being much broader than at 50° . The slope of the reddening line is 2.00 ± 0.14 .

Table 2. The investigated areas located in star-forming areas. The given mean ratios of color excesses correspond to $J-H$ between 1.6–2.2 for most areas, but between 1.2–2.0 in the Lup 1 cloud. The last column shows the number of stars used to calculate the ratio of color excesses.

Area	Number in Dobashi et al. (2005)	Center		E_{J-H}/E_{H-K_s}	Number of stars
		ℓ°	b°		
Ser core	T 289-P12	31.6	+5.3	2.096 ± 0.215	62
Ser cloud	T 279-P7	28.8	+3.5	1.983 ± 0.165	502
Ser cloud	T 243-P1/2	23.5	+8.3	2.052 ± 0.188	65
Pipe nebula	T 25-P1	1.6	+3.4	1.912 ± 0.206	908
CrA cloud	T 2213-P1/2	359.9	-17.8	1.787 ± 0.160	9
Pipe nebula	Barnard 59	357.2	+7.1	1.925 ± 0.176	92
Oph cloud lane	T 2171-P1,	354.0	+15.8	1.934 ± 0.135	65
Oph cloud lane	T 2171-P5,	354.9	+15.0	–	–
Rho Oph cloud	T 2171-P3	353.0	+17.0	1.915 ± 0.177	50
Lup1 cloud	T 2072	338.0	+16.4	2.087 ± 0.221	18
Lup1 cloud	T 2079-P1/2	338.8	+17.4	–	–
Lup3 cloud	T 2084	339.5	+9.3	1.900 ± 0.165	19

4.4. Two-color diagrams for the Gould Belt areas containing dense dust clouds

In Figure 6 (a–j) we present the $J-H$ vs. $H-K$ diagrams for some areas of the Local arm located towards the inner Galaxy (Table 2). Most of them are known star-forming regions within the Gould Belt. The slopes of the reddening lines of red giants were calculated for the stars with $J-H$ between 1.6 and 2.2. In the Lupus areas this interval was 1.2–2.0. As in the case of the Galactic plane areas, we have excluded possible AGB stars and YSOs located below the reddening line of red giants with the slope 1.6.

4.4.1. The Serpens dust/molecular cloud

In our investigation the direction to the Serpens section of the Aquila Rift is represented by three areas, coinciding with the dust clumps T 289-P12, T 279-P7 and T 243-P1/2 in the Dobashi et al. (2005) atlas. The $J-H$ vs. $H-K_s$ diagrams for stars in these three areas are plotted in Figures 6 (a), (b) and (c). The Serpens clouds are at a distance of about 225 pc (Straizys et al. 1996, 2003). Most probably, in the direction of the first and the third areas this is the only dust layer in the line of sight. In this case the distribution of distant red clump giants and of cooler K and M giants along the reddening line is caused by a differential reddening originating in this single layer. The second Serpens area is at lower Galactic latitude ($b = +3.5^\circ$), and the line of sight can cross more dust clouds at larger distances. This area has the largest surface density of dust with the maximum extinction A_V of 28 mag, while in the first and the third area the extinction is about 20 and 15 mag, respectively. In all diagrams the stars lying lower than the reddening line of red giants are observed. Their possible origin was discussed in Section 3.

In all three diagrams we observe the rise of density of red giants at $J-H \approx 1.0$, which corresponds to $A_V = 3.4$. Although the lengths of reddening lines in the three directions are quite different, their slopes are similar: the stars are scattered between the color-excess ratios of 1.8 and 2.1, the mean values of slopes being 2.10 ± 0.21 , 1.98 ± 0.16 and 2.05 ± 0.19 (Table 2).

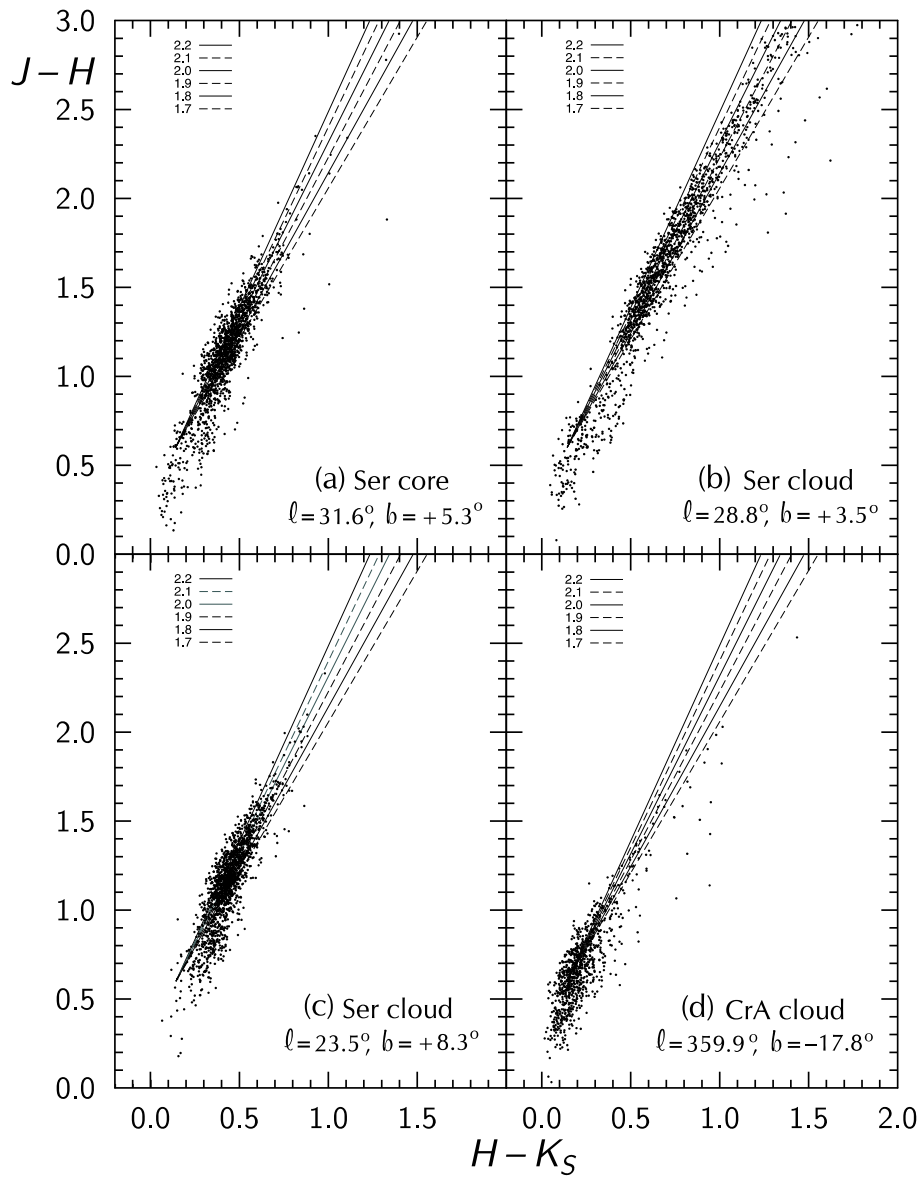


Fig. 6 (a-d). Two-color diagrams for the star-forming areas: (a) – the Serpens cloud core, (b) and (c) – two Serpens cloud areas and (d) – the CrA cloud. The six straight lines are the reddening lines of RCGs with different slopes, explained in the inserts.

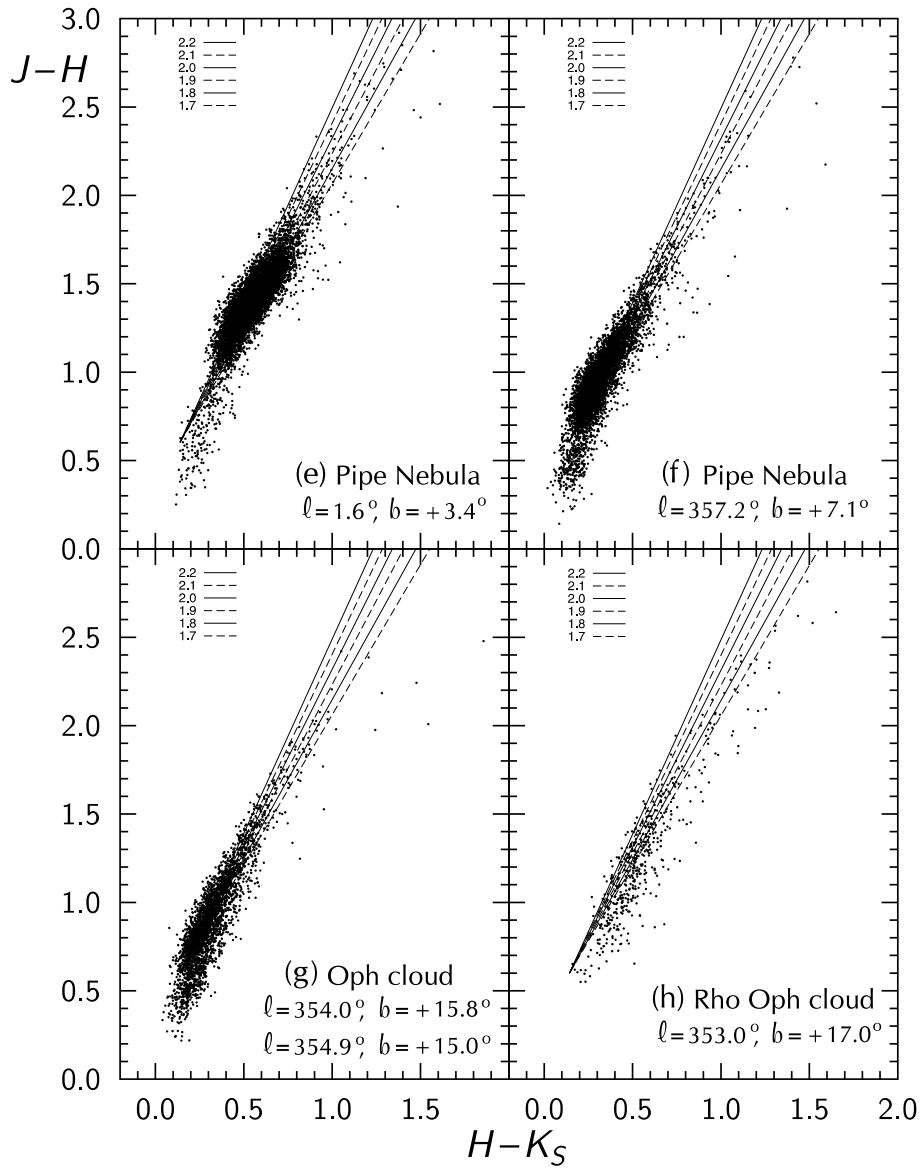


Fig. 6 (e-h). The same as in Fig. 6 (a-d) but for the areas: (e) and (f) – two areas in the Pipe Nebula, (g) – two areas in a dark lane of the Rho Ophi cloud and (h) – the central Rho Ophi cloud area.

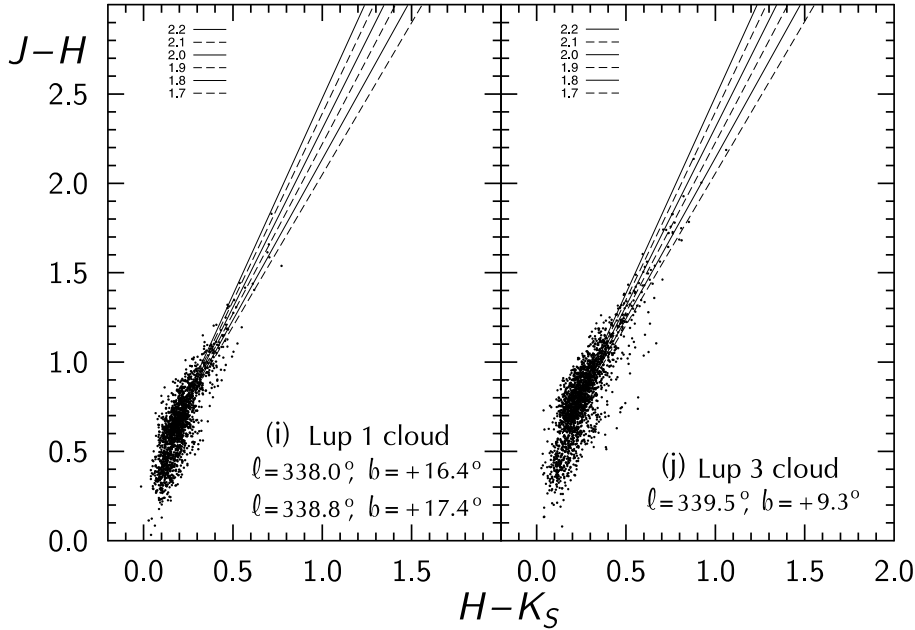


Fig. 6 (i–j). The same as in Fig. 6 (a–d) but for the areas: (i) – two areas in the Lupus 1 cloud and (j) – an area in the Lupus 3 cloud.

4.4.2. The Corona Australis dust/molecular cloud

This cloud with active star formation is represented by the area in its densest place with the center at $\ell = 359.9^\circ, b = -17.8^\circ$. The most recent review of the region by Neuhäuser & Forbrich (2008) places the cloud at a distance of 130 pc. Its reddening line of red giants in the $J-H$ vs. $H-K_s$ diagram (Figure 6d) has its end probably at $J-H \approx 2.0$; this corresponds to $A_V = 11.9$ mag. The reddening line of red giants from below has a well populated sequence of pre-main-sequence stars. Although it is difficult to find the boundary of the two sequences, between $J-H = 1.0$ and 1.6 the reddening line of red giants is sufficiently well defined. The mean slope of 9 stars falling between $J-H = 1.6$ and 2.0 is 1.79 ± 0.16 , i.e., it is somewhat smaller than in most of other areas described in Sections 4.3 and 4.4.

4.4.3. The Pipe Nebula

The Pipe Nebula dark cloud in the direction of the Galactic center is located at a distance of about 130 pc and belongs to the Scorpio-Centaurus subsystem of the Gould Belt (see the review by Alves et al. 2008). This dark cloud is represented by two areas at Galactic latitudes $+3.4^\circ$ and $+7.1^\circ$. Since both areas are out of Galactic plane, the giants located at various distances and seen in the background all are reddened only by the Pipe Nebula cloud. As a result, CMDs in this direction are quite similar to the CMD for Baade's Window shown in Figure 4a: in the diagrams the giants located at various distances form a broad belt extending from $K_s \approx 8.0$ to 13.0. However, the reddening in the Pipe areas is larger than in Baade's Window. In the first and the second Pipe areas the lower end of the belt is at $(K_s, H-K_s) = (13.0, 0.45)$ and $(13.0, 0.25)$, respectively.

In the $J-H$ vs. $H-K_s$ diagram (Figures 6e and 6f) the giant sequences representing the Pipe Nebula are very rich but most stars are lower than $J-H = 1.5$ or 2.0, respectively. At large reddenings only a few stars are present. The mean slopes of the reddening lines at $J-H = 2.0$ in the two areas are 1.91 ± 0.21 and 1.92 ± 0.18 , respectively.

4.4.4. The Rho Ophiuchi and related clouds

The Rho Ophiuchi star-forming region, located at a distance of 120–140 pc (Wilking et al. 2008) in our sample is represented by three areas: one of them is placed on the densest part of the Rho Oph cloud and the remaining are located on the dust lane extending in the direction of the bulge. Since in the last two areas the density of heavily reddened stars is rather low, in the $J-H$ vs. $H-K_s$ diagram (Figure 6g) we plotted stars from both these areas together. The diagram for the Rho Oph area is plotted separately (Figure 6h). Red giants with $J-H$ between 1.6 and 2.2 in both diagrams follow the reddening lines with the mean slopes 1.93 ± 0.14 and 1.92 ± 0.18 .

4.4.5. The Lupus clouds

For the investigation of the Lupus cloud area we selected three dust clumps: two of them are in the Lupus 1 cloud and one is in the Lupus 3 cloud. According to Comerón (2008), the Lupus 1 cloud is located at a distance of ~ 150 pc and the Lupus 3 cloud at ~ 200 pc. To increase the number of heavily reddened stars, the stars from both areas of the Lupus 1 cloud were plotted on the same graph (Figure 6i). Even in this case the most reddened stars are lower than in other areas. The slope of reddening line derived from 18 stars between $J-H = 1.2$ and 1.8 is 2.09 ± 0.22 . In the Lupus 3 cloud (Figure 6j) the maximum reddening is much larger. However, here is a clear dependence of the slope on the minimum value of $J-H$. Taking 19 stars between $J-H = 1.6$ and 2.2 we obtain the slope 1.90 ± 0.16 . However, taking 70 stars between $J-H = 1.25$ and 2.2 the slope is 2.00 ± 0.25 . Probably, at the largest reddenings we encounter the influence of YSOs.

5. DISCUSSION

In this section we compare our results with the reddening line slopes obtained in the same range of Galactic coordinates in other investigations. To avoid systematic errors, we will take into account only those studies which are based on the J, H, K_s photometric data taken from the 2MASS survey or obtained by special observations in similar photometric systems.

To our knowledge, no systematic investigations of reddening effects in the 2MASS $J-H$ vs. $H-K_s$ diagram along the Milky Way have been undertaken so far. However, star-forming regions of the Local arm, seen in the direction of inner Galaxy, were investigated in many papers.

Let us start from the direction toward the Galactic bulge. Recently, two investigations of the reddening law in infrared were published by Nishiyama et al. (2006, 2008). The authors have used deep J, H, K_s photometry in the SIRIUS photometric system obtaining $E_{J-H}/E_{H-K_s} = 1.72$ and 1.74. However, the SIRIUS system is different from the 2MASS system (Kato et al. 2007; Kućinskas et al. 2008). After reduction of the Nishiyama et al. colors to the 2MASS system, we obtain the color-excess ratio close to 2.0.

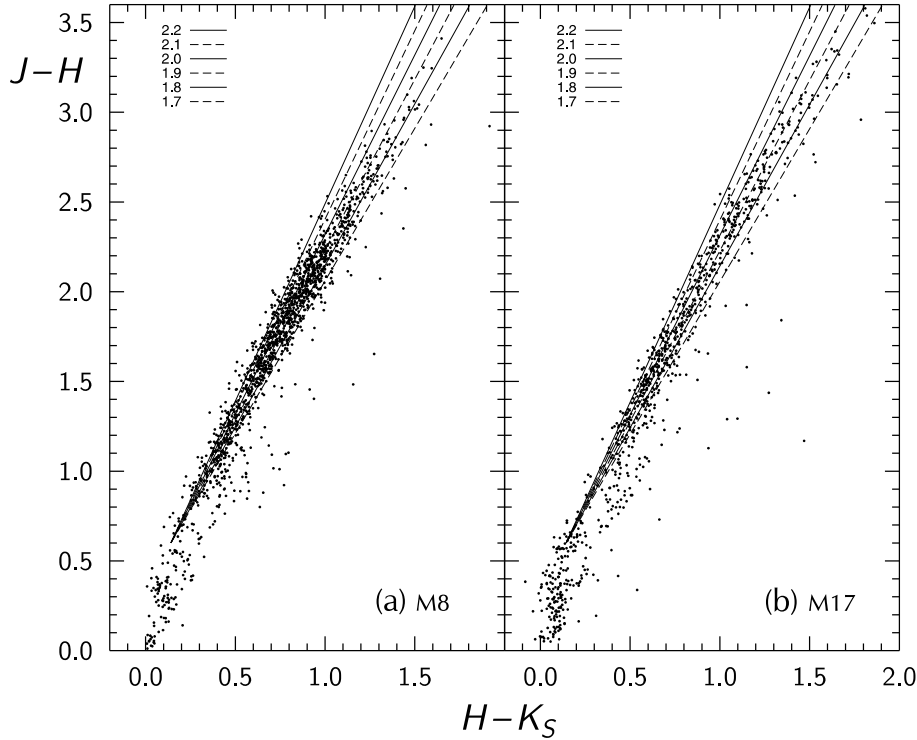


Fig. 7. The same as in Figure 6 but for the areas: (a) – M8 (Lagoon Nebula) and (b) – M17 (Omega Nebula).

In two other papers 2MASS data have been used to investigate the reddening in the direction of the Pipe Nebula, including the dark cloud B 59. Lombardi et al. (2006) in a large area of $8^\circ \times 6^\circ$ find that the ratio $E_{J-H}/E_{H-K_s} = 1.85 \pm 0.15$. Brooke et al. (2007) in their *Spitzer* project “Cores to Disks” for the B 59 cloud show the $J-H$ vs. $H-K_s$ diagram with the reddening line having a slope of 1.92. An extremely low value of the slope, 1.36–1.52, has been obtained by Román-Zúñiga et al. (2007) in their investigation of the extinction law in the core of the B 59 cloud. Most probably, this result can be explained by the ignorance of the band-width effect, i.e., the curvature of the reddening line. As it is shown by Straižys & Lazauskaitė (2008), this effect is quite strong at heavy reddenings.

Arias et al. (2006) in the J, H, K_s system investigated the Hourglass Nebula within the Lagoon Nebula (M 8) at $\ell = 6.0^\circ$, $b = -1.2^\circ$ from the images obtained at the Las Campanas Observatory. Although the authors accept a slope of the reddening line from Rieke & Lebofsky (1985), the distribution of the reddened field stars in the $J-H$ vs. $H-K_s$ diagrams for the Hourglass Nebula and the nearby control field are consistent with a higher slope of 1.9–2.0. In Figure 7a we show the $J-H$ vs. $H-K_s$ diagram plotted for an area with a diameter of 0.5° in the direction of M 8 for stars with the accuracy of 2MASS magnitudes of ≤ 0.03 mag. The mean ratio of color excesses for 332 stars with $J-H$ between 1.8 and 2.2 is 1.97 ± 0.16 .

Two J, H, K_s investigations in the M17 region (Omega Nebula) at $\ell = 15^\circ$,

$b = -0.7^\circ$ are available. Jiang et al. (2002) using the SIRIUS system obtain the reddening line slope of 1.9. Hoffmeister et al. (2008) from imaging observations on VLT in another area of M17 obtain the ratio 2.06. Unfortunately, photometric systems of both investigations are not sufficiently described, so we are not sure if these ratios are valid for the 2MASS system. In Figure 7b we plot the stars in the direction of M17 taking 2MASS magnitudes with an accuracy of ≤ 0.03 mag. The mean ratio of color excesses for 111 stars with $J-H$ between 1.8 and 2.2 is 1.96 ± 0.15 .

The star-forming complex Rho Ophiuchi was long known as the region with a low ratio of E_{J-H}/E_{H-K} (1.57, Kenyon et al. 1998; 1.60–1.68, Naoi et al. 2006). The determination of the RCG reddening line slope in this region is complicated by abundant population of YSOs which in the $J-H$ vs. $H-K_s$ diagram lie lower than red giants. However, YSOs are less abundant in the dark lanes extending from the central Rho Ophiuchi cloud. Our Figure 6h representing the clumps P1 and P5 of the T 2171 cloud shows that at $J-H = 2.0$ the slope of the RCG line is consistent with values between 1.7 and 2.1, the average slope being 1.93 ± 0.14 . A similar slope can be derived from Fig. 5 of Lombardi et al. (2008) plotted from the 2MASS data (including the observations with lower accuracy) for a large region covering Ophiuchus and Lupus.

Haas et al. (2008) plotted the $J-H$ vs. $H-K_s$ diagram for the R Coronae Australis cloud stars imaged with the CTIO 4 m Blanco telescope and obtained a slope of 1.8. This value is consistent with our diagram shown in Figure 6d, if we exclude possible pre-main-sequence objects. In Table 2 we give a value of 1.79 ± 0.16 .

Indebetouw et al. (2005) included the region at $\ell = 42^\circ$, $b = +0.5^\circ$ in Aquila in the investigation of the infrared interstellar extinction law. Their value of $E_{J-H}/E_{H-K_s} = 1.78$ based on the 2MASS data is not very different from our estimate at $\ell = 40^\circ$ (1.98 ± 0.16 , Figure 5c).

6. CONCLUSIONS

The results of this investigation allow us to conclude that in the direction of the inner Galaxy, between the longitudes 60° and 310° , the ratio E_{J-H}/E_{H-K_s} of red giants shows quite small variations. The value of the ratio measured for red giants at $J-H \approx 2.0$ is between 1.9 and 2.0 both in the clouds of the Local arm and in the Sagittarius arm. The Galactic bulge red giants reddened by interstellar clouds of the Local, Sagittarius, Scutum, Norma and 3-kpc arms also follow the same reddening law. In the 2MASS system the ‘normal’ value of the ratio probably is close to 1.9–2.0, i.e., it is larger by 0.2–0.3 than it was usually considered modeling the interstellar dust.

Most values of E_{J-H}/E_{H-K_s} reported till now in the literature, except for a few exclusions, are between 1.6–1.8, i.e., they are lower than the values obtained above. We conclude that the reduction of the observed ratios can be conditioned by several reasons: (1) the ignorance of the fact that interstellar reddening lines in the $J-H$ vs. $H-K_s$ diagrams are not straight but due to the band-width effect at large reddenings they bend down; (2) in the areas near the Galactic equator and towards the bulge most luminous and most reddened stars are oxygen- or carbon-rich AGB stars whose intrinsic positions in the $J-H$ vs. $H-K_s$ diagram bend down from the intrinsic sequence of K–M5 giants; (3) in some star-forming areas the slope of the reddening line can be reduced by unrecognized young stellar

objects (YSOs) in various stages of evolution; many of them are surrounded by warm dust envelopes and disks which place them in the $J-H$ vs. $H-K_s$ diagram lower than the reddening line of RCGs.

One more source of disagreement between different determinations of color-excess ratios in the same area is related to the variety of photometric systems used, even if they all have the same designation (J , H , K_s). The observers in some cases use only a few standard stars with their magnitudes imported from other (similar) photometric system, without any color corrections. Other sources of significant systematic errors can be related to insufficient atmospheric extinction corrections (average extinction coefficients accepted), response non-linearity of the detectors, inhomogeneities in the filter transmittance curves, etc. All these effects should be carefully taken into account.

ACKNOWLEDGMENTS. We are grateful to Edmundas Meistas for his help preparing the figures. The use of the 2MASS, SkyView and Simbad databases is acknowledged.

REFERENCES

- Alves D. R. 2000, ApJ, 539, 732
 Alves J., Lombardi M., Lada Ch. J. 2008, in *Handbook of Star Forming Regions*, vol. 2, ed. B. Reipurth, ASP, p.415
 Arias J. I., Barbá R. H., Maíz Appellániz J. et al. 2006, MNRAS, 366, 739
 Benjamin R. A. et al. 2008, BAAS, 40, 266; NASA News, June 3, 2008
 Brooke T. Y., Huard T. L., Bourke T. L. et al. 2007, ApJ, 655, 364
 Comerón F. 2008, in *Handbook of Star Forming Regions*, vol. 2, ed. B. Reipurth, ASP, p. 295
 Cotera A. S., Simpson J. E., Erickson E. F. et al. 2000, ApJS, 129, 123
 Cutri R. M., Skrutskie M. F., Van Dyk S., Beichman C. A. et al. 2006, Explanatory Supplement to the 2MASS All Sky Data Release and Extended Mission Products,
<http://www.ipac.caltech.edu/2mass/releases/allsky/doc/explsup.html>
 Dutra C. M., Santiago B. X., Bica E. 2002, A&A, 381, 219
 Dutra C. M., Santiago B. X., Bica E. L D., Barbuy B. 2003, MNRAS, 338, 253
 Eiroa C., Djupvik A. A., Casali M. M. 2008, in *Handbook of Star Forming Regions*, vol. 2, ed. B. Reipurth, ASP, p.693
 Forbes D. 1985, AJ, 90, 301
 Frogel J. A., Tiede G. P., Kuchinski L. E. 1999, AJ, 117, 2296
 Grocholski A. J., Sarajedini A. 2002, AJ, 123, 1603
 Groenewegen M. A. T. 2008, A&A, 488, 935
 Haas M., Heymann F., Domke I. et al. 2008, A&A, 488, 987
 Hoffmeister V. H., Chini R., Scheyda C. M. et al. 2008, ApJ, 686, 310
 Indebetouw R., Mathis J. S., Babler B. L. et al. 2005, ApJ, 619, 931
 Jiang Z., Yao Y., Yang J. et al. 2002, ApJ, 577, 245
 Kato D., Nagashima C., Nagayama T. et al. 2007, PASJ, 59, 615
 Kenyon S. J., Lada E. A., Barsony M. 1998, AJ, 115, 252
 Kučinskas A., Dobrovolskas V., Lazauskaite R., Lindegren L., Tanabe T. 2008, Baltic Astronomy, 17, 283 (this issue)
 Lombardi M., Alves J., Lada C. J. 2006, A&A, 454, 781

- Lombardi M., Lada C. J., Alves J. 2008, *A&A*, 489, 143
- Naoi T., Tamura M., Nakajima Y. et al. 2006, *ApJ*, 640, 373
- Neckel Th., Klare G. 1980, *A&AS*, 42, 251
- Neuhäuser R., Forbrich J. 2008, in *Handbook of Star Forming Regions*, vol. 2, ed. B. Reipurth, ASP, p. 735
- Nishiyama S., Nagata T., Kusakabe N. et al. 2006, *ApJ*, 638, 839
- Nishiyama S., Nagata T., Tamura M. et al. 2008, *ApJ*, 680, 1174
- Prato L., Rice E. L., Dame T. M. 2008, in *Handbook of Star Forming Regions*, vol. 1, ed. B. Reipurth, ASP, p. 18
- Racca G., Gómez M., Kenyon S. J. 2002, *AJ*, 124, 2178
- Rieke G. H., Lebofsky M. J. 1985, *ApJ*, 288, 618
- Román-Zúniga C. G., Lada C. J., Muench A., Alves J. F. 2007, *ApJ*, 664, 357
- Schultheis M., Ganesh S., Simon G. et al. 1999, *A&A*, 349, L69
- Schultheis M., Glass I. S. 2001, *MNRAS*, 327, 1193
- Skrutskie M. F., Cutri R. M., Stiening R., Weinberg M. D. et al. 2006, *AJ*, 131, 1163
- Straizys V., Černis K., Bartašiūtė S. 1996, *Baltic Astronomy*, 5, 125
- Straizys V., Černis K., Bartašiūtė S. 2003, *A&A*, 405, 585
- Straizys V., Corbally C. J., Laugalys V. 2008, *Baltic Astronomy*, 17, 125
- Straizys V., Lazauskaitė R. 2008, *Baltic Astronomy*, 17, 277 (this issue)
- Tiede G. P., Frogel J. A., Terndrup D. M. 1995, *AJ*, 110, 2788
- Wilking B. A., Gagné M., Allen L. E. 2008, in *Handbook of Star Forming Regions*, vol. 2, ed. B. Reipurth, ASP, p. 351